

One Dimensional Kondo Lattice Model Studied by the Density Matrix Renormalization Group Method

Naokazu Shibata

Institute of Applied Physics, University of Tsukuba, Tsukuba 305, Japan

Kazuo Ueda

Institute for Solid State Physics, University of Tokyo, 7-22-1 Roppongi, Minato-ku, Tokyo 106-8666, Japan

(April 3, 2018)

Recent developments of the theoretical investigations on the one-dimensional Kondo lattice model by using the density matrix renormalization group (DMRG) method are discussed in this review. Short summaries are given for the zero-temperature DMRG, the finite-temperature DMRG, and also its application to dynamic quantities.

Away from half-filling, the paramagnetic metallic state is shown to be a Tomonaga-Luttinger liquid with the large Fermi surface. For the large Fermi surface its size is determined by the sum of the densities of the conduction electrons and the localized spins. The correlation exponent K_ρ of this metallic phase is smaller than 1/2. At half-filling the ground state is insulating. Excitation gaps are different depending on channels, the spin gap, the charge gap and the quasiparticle gap. Temperature dependence of the spin and charge susceptibilities and specific heat are discussed. Particularly interesting is the temperature dependence of various excitation spectra, which show unusual properties of the Kondo insulators.

I. INTRODUCTION

In a degenerate Fermi gas, low temperature specific heat is linear in T and the proportionality constant is given by the density of states at the Fermi energy. For the free electrons the density of states including the two spin directions is given by

$$D(\epsilon_F) = \frac{mk_F}{\pi^2 \hbar^2} \quad (1)$$

where m is the free electron mass and k_F is the Fermi wave number.

To include the effect of electron-electron interaction, Landau developed the theory of Fermi liquids. Since the volume of the Fermi sphere is determined by the density of electrons, it is a reasonable assumption that the Fermi wave number does not change by the interaction, which was in fact proven later by Luttinger [1]. According to Landau, the effect of the interaction can be taken into account by replacing the bare electron mass m by an effective mass m^* . Thus importance of the interaction effects in each material may be judged from the electronic specific heat at low temperatures.

In ordinary metals the coefficient of the T -linear term, γ , is of the order of mJ/mol K^2 . However, in some rare earth and actinide compounds there is a group of compounds whose γ are in the range from 0.1 J/mol K^2 to more than 1 J/mol K^2 . This class of materials are called heavy Fermion systems or heavy electron systems. A key feature of the heavy Fermion systems is that it contains two different types of electrons: relatively localized f electrons and extended conduction electrons. Interplay between the two degrees of freedom is an essence of the heavy Fermion physics.

Since the Coulomb interaction between the f electrons is strong, a partially filled f shell in an isolated ion possesses a well defined magnetic moment corresponding to the total angular momentum of the f shell. A weak hybridization between the f electrons and the conduction electrons is the source of interesting manybody problems.

When we consider a single f shell in the sea of conduction electrons, the magnetic moment of the f electrons is unstable, leading to the Kondo singlet which is a bound state of the f moment with the spin polarization of the conduction electrons [2]. When we consider two f shells, spin polarization of the conduction electrons induced by an f moment tends to stabilize the magnetic moment of the other f shell. This is the origin of the Ruderman-Kittel-Kasuya-Yosida (RKKY) interaction [3]. Thus the Kondo effect and the RKKY interaction in many cases compete with each other.

If the Kondo effect dominates over the RKKY interaction by some reason, a paramagnetic heavy Fermion state will be stabilized. In this regime, the Kondo temperature or the effective Fermi temperature in a lattice problem sets a small energy scale at low temperatures. Existence of the small energy scale naturally leads to the large specific heat since the entropy associated with the magnetic degrees of freedom of f orbitals should be released in the small temperature range.

The most simple theoretical model for the heavy Fermion physics is the Kondo lattice model. The Kondo lattice model is given by

$$\mathcal{H} = \sum_{\langle ij \rangle} \sum_s t_{ij} c_{is}^\dagger c_{js} + J \sum_i \sum_{s,s'} \vec{S}_i \cdot \frac{1}{2} \vec{\sigma}_{ss'} c_{is}^\dagger c_{is'} \quad (2)$$

where $\vec{\sigma} = (\sigma_x, \sigma_y, \sigma_z)$ are the Pauli matrices and $\vec{S}_i =$

$\sum_{s,s'} \frac{1}{2} \vec{\sigma}_{ss'} f_{is}^\dagger f_{is'}$ is the f -electron spin at site i . In this review we will consider the model with only nearest neighbor hoppings, $t_{ij} = -t$ for the nearest neighbor pairs.

Much effort has been invested for the study of the model and a significant progress has been achieved in one dimension in the last ten years [4]. When we fix a lattice structure, the Kondo lattice model has only two parameters: one is the density of conduction electrons n_c and the other is the strength of the exchange coupling normalized by the hopping energy J/t . In one dimension, the ground-state phase diagram in the parameter space is completed and shown in Fig. 1.

There are three different phases in the phase diagram. In the region from the low density limit to the strong coupling limit, a ferromagnetic metallic phase is stabilized. The spin quantum number in this phase is given by $S_{\text{tot}} = (L - N_c)/2$, where L is the number of lattice sites and N_c the number of conduction electrons. Note that the magnetic moment vanishes as the half-filling is approached. The line of half-filling is special in the sense that the ground state is always a nonmagnetic insulator. Since the lowest excitation in this phase is a spin-triplet excitation with a finite excitation gap, this phase is called an incompressible spin liquid phase. In the remaining part of the phase diagram (Fig.1) which extends from the weak coupling limit towards the line of half-filling, the ground state is metallic and paramagnetic. In this review we will discuss properties of the spin liquid phase and the paramagnetic metallic phase.

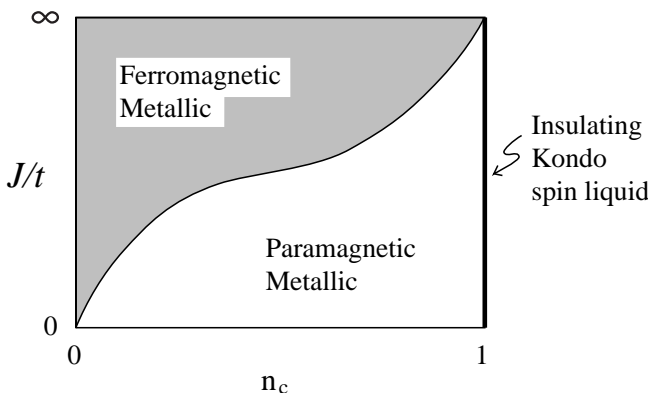


FIG. 1. The ground-state phase diagram of the one dimensional Kondo lattice model with the nearest neighbor hoppings.

Existence of the small energy scale in the Kondo lattice model means that correlation lengths are generally long. For example, to study the spin gap and the charge gap in the spin liquid phase the exact diagonalization was used at first [5]. However the largest system size which can be diagonalized by the Lanczos algorithm is just ten sites. This is the reason why a nontrivial form of a finite size scaling was necessary to obtain the functional form of the spin gap.

Recently Steven White developed the density matrix

renormalization group (DMRG) method to study the ground-state properties of one dimensional many body systems [6]. Advantage of this method is that an order of magnitude bigger systems can be studied compared with the numerical exact diagonalization by the Lanczos algorithm. Compared with quantum Monte Carlo simulations the DMRG is free from statistical errors. The numerical errors in the DMRG come from truncation errors but they can be estimated from the largest eigenvalue of the density matrix which is truncated out. The truncation error may be improved by increasing the number of basis states for the density matrix. The DMRG method is an ideal tool to study the one-dimensional Kondo lattice model and in this review we will discuss recent developments on this subject.

Further development of the DMRG method was achieved last year when one of the authors [7] and Wang and Xiang [8] independently succeeded to obtain thermodynamic properties of the one-dimensional quantum XXZ model by applying the DMRG to the transfer matrix (finite- T DMRG). Application of the finite- T DMRG to a system with Fermion degrees of freedom started from the Kondo lattice model [9].

The present article is organized as follows. In the next section, after a brief summary of the DMRG method for the ground state, we will describe the method to calculate thermodynamic properties by the finite- T DMRG and then extend discussions to the dynamic quantities at finite temperatures. In Section III nature of the paramagnetic metallic phase away from half-filling is shown to be a Tomonaga-Luttinger liquid with a large Fermi surface. The large Fermi surface means that the volume inside the Fermi surface is determined not only by the density of conduction electrons but also includes the localized spins. Section IV is devoted to the discussion of the spin liquid phase at half-filling. After the discussion of the spin gap and the charge gap at zero temperature, we will discuss how the excitation gaps develop as the temperature is lowered. We will conclude the present review by summary and discussions in Section V.

II. THE DENSITY MATRIX RENORMALIZATION GROUP METHOD

The density matrix renormalization group (DMRG) method is relatively new [6] among the various numerical algorithms to treat many-body problems. However it is now widely used as one of the most standard numerical methods for low dimensional many-body systems. In this section we first briefly outline the algorithm of the zero-temperature DMRG that was developed to study ground-state and low energy excitations of one-dimensional systems. The application of this method to the quantum transfer matrix enables us to obtain thermodynamic quantities [7,8] and the dynamical correlation functions at finite temperatures. In the second part

of this section we will summarize the algorithm of the finite- T DMRG.

A. Zero temperature algorithm

The zero-temperature DMRG method is designed to obtain the ground-state wave function and the low energy excitations with small systematic errors. The ground-state wave function and the low energy excitations of long systems are obtained by expanding the system size iteratively as shown in Fig. 2. The expansion of the system is done by putting additional sites in its central region to minimize undesirable boundary effects on the added sites. The algorithm is described in the following.

Let us start from a system of four identical sites, for example, a four-sites spin chain under the open boundary conditions. An operator on the n th site, e.g. S_n , is represented in terms of the complete basis states $|i_n\rangle$ as

$$\langle i_n | S_n | i'_n \rangle = (S_n)_{i_n, i'_n}. \quad (3)$$

Then we construct a representation of the Hamiltonian $H_{i_1 i_2 i_3 i_4, i'_1 i'_2 i'_3 i'_4}$ for the total system. The ground-state eigenvector

$$|\Psi_{i_1 i_2 i_3 i_4}\rangle = \Psi_{i_1 i_2 i_3 i_4} |i_1\rangle |i_2\rangle |i_3\rangle |i_4\rangle \quad (4)$$

is obtained by diagonalizing the Hamiltonian matrix by some method like the Lanczos algorithm. Then $\Psi_{i_1 i_2 i_3 i_4}$ is used to construct the density matrix

$$\rho_{i_1 i_2, i'_1 i'_2} = \sum_{i_3 i_4} \Psi_{i_1 i_2 i_3 i_4} \Psi_{i'_1 i'_2 i_3 i_4}^* \quad (5)$$

for the block containing the sites $n = 1$ and 2. The density matrix specifies to what extent the basis states $|i_1\rangle |i_2\rangle$ of the block are contributing to the total wave function $|\Psi_{i_1 i_2 i_3 i_4}\rangle$. This matrix is numerically diagonalized, and we obtain its eigenvalues λ^α and eigenvectors $v_{i_1 i_2}^\alpha$. Then we select the eigenvectors of the largest m eigenvalues as new basis states for the block. Here m is the number of the basis states kept for the block at the next step. Using the selected eigenvectors of the density matrix we represent the operators on the site, for example, $n = 2$ as

$$(S_2)_{\alpha, \alpha'} = \sum_{i_1 i_2 i'_2} (S_2)_{i_2, i'_2} (v_{i_1 i_2}^\alpha)^* v_{i_1 i'_2}^{\alpha'}. \quad (6)$$

A similar procedure is repeated for the block of the sites $n = 3$ and 4, and all operators in the original system are represented in terms of the new basis states

$$|\alpha\rangle = \sum_{i_1 i_2} v_{i_1 i_2}^\alpha |i_1\rangle |i_2\rangle, \quad (7)$$

$$|\beta\rangle = \sum_{i_3 i_4} v_{i_3 i_4}^\beta |i_3\rangle |i_4\rangle. \quad (8)$$

To increase the size of system we introduce two new sites between the blocks $n = 1, 2$ and $n = 3, 4$. Using the basis states $|i_2'\rangle$ and $|i_3'\rangle$, for the new sites, we construct the Hamiltonian matrix of the expanded system $H_{\alpha i_2, i_3' \beta, \alpha' i'_2, i'_3 \beta'}$. Renaming the indices as

$$\alpha \rightarrow i_1, i_2' \rightarrow i_2, i_3' \rightarrow i_3, \beta \rightarrow i_4, \quad (9)$$

we repeat the procedures from the diagonalization of the Hamiltonian matrix.

The key feature of the above renormalization procedure is that the new basis states $|\alpha\rangle$ or $|\beta\rangle$ of each block contain the information that the block is a part of the total system. As shown in Fig. 2 the edge part of each block connecting to the remaining part of the system is located in the middle of the system, and this part is not so sensitive to the boundary conditions imposed on the total system. Thus we expect that the new basis states also dominantly contribute to the ground-state wave function of the expanded system which has two additional sites in the middle of the two blocks.

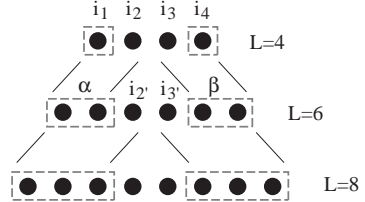


FIG. 2. Schematic diagram of the infinite system algorithm of the DMRG.

The above algorithm is called the infinite system algorithm of the DMRG. Using this algorithm we increase the size of the system. In order to improve the basis states of the blocks, it is necessary to fix the size of system and use the following algorithm which is known as the finite system algorithm of the DMRG. The schematic diagram of the finite system algorithm is shown in Fig. 3.

Let us take a block of size $n - 1$ on the left and another block of size $n - 1$ on the right whose basis states are represented by $|v_{L(n-1)}^i\rangle$ and $|v_{R(n-1)}^i\rangle$. These basis states and representations of the operators in the blocks are obtained after the $(n - 2)$ th renormalization step from the initial four-site system. The system of size $2n$ is constructed by inserting additional two sites for which the basis states are represented by $|i_{L'}\rangle$ and $|i_{R'}\rangle$.

We again diagonalize the Hamiltonian matrix of this $2n$ -site system $H_{i_{L(n-1)} i_{L'} i_{R(n-1)} i'_{L(n-1)} i'_{L'} i'_{R(n-1)}}$ and obtain the ground-state wave function $\Psi_{i_{L(n-1)} i_{L'} i_{R(n-1)} i'_{R(n-1)}}$. Then construct the density matrix

$$\rho_{i_{L(n-1)} i_{L'}, i'_{L(n-1)} i'_{L'}} = \sum_{i_{R'} i_{R(n-1)}} \Psi_{i_{L(n-1)} i_{L'} i_{R'} i_{R(n-1)}} \Psi_{i'_{L(n-1)} i'_{L'} i'_{R'} i_{R(n-1)}}^* \quad (10)$$

for the subspace spanned by $|v_{L(n-1)}^i\rangle$ and $|i_{L'}\rangle$. We use the m important eigenvectors of this density matrix as a new basis states of the block containing n sites, and represent all operators in the new block in terms of the new basis states.

In the next step, we take the new left block with n sites and the right block with $n - 2$ sites. The right block with $n - 2$ sites has been obtained at the $(n - 3)$ th renormalization step from the initial four-site system. Inserting two sites between these blocks, we construct the Hamiltonian matrix of the total system $H_{i_{L(n)}i_{L'}i_{R'}i_{R(n-2)}, i'_{L(n)}i'_{L'}i'_{R'}i'_{R(n-2)}}$, and repeat above all procedures.

We continue to increase (decrease) the size of the left (right) block until the right block is reduced to the single site. Then we turn to decrease (increase) the size of the left (right) block in order to improve the basis states of the right block. We continue to decrease (increase) the size of the left (right) block until the left block is reduced to the single site. These procedures are continued back and forth until we get a good convergence.

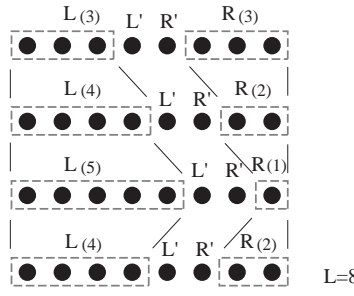


FIG. 3. Schematic diagram of the finite system algorithm of the DMRG.

In general, the total energy of the system is lowered as the basis states of the blocks are reconstructed. Thus, the lowest energy is obtained after the convergence. The wave function obtained by the finite system algorithm of the DMRG method may be represented by a matrix product form [10]. Therefore the finite system algorithm of the DMRG method is considered to be a numerical variational method which uses the matrix product wave function. This is another reason why we can get remarkable accuracy by the DMRG method. The accuracy of the ground-state energy and the wave function is determined by the eigenvalues of the density matrix which are truncated out. Thus we can improve the accuracy by increasing the number of basis states m used in the calculations so long as the memory of computer allows.

B. Finite temperature algorithm

It is also possible to discuss thermodynamic quantities by the DMRG method, finite- T DMRG. The readers who

are not interested in the detail of the iteration procedures may skip the paragraph including Eqs. (13) to (26). In this method we use the quantum transfer matrix defined as

$$\begin{aligned} \mathcal{T}_{n(M)} &= [e^{-\beta h_{2n-1,2n}/M} e^{-\beta h_{2n,2n+1}/M}]^M \\ &= \sum_{\sigma_{2n\tau_1}} \sum_{\sigma_{2n\tau_1}} \sum_{\sigma_{2n\tau_2}} \cdots \sum_{\sigma_{2n\tau_M}} \sum_{\sigma_{2n\tau_M}} \\ &\quad \langle \sigma_{2n-1,\tau_1} \sigma_{2n-1,\tau_1} | e^{-\beta h_{2n-1,2n}/M} | \sigma_{2n,\tau_1} \sigma_{2n,\tau_1} \rangle \\ &\quad \langle \sigma_{2n,\tau_1} \sigma_{2n,\tau_2} | e^{-\beta h_{2n,2n+1}/M} | \sigma_{2n+1,\tau_1} \sigma_{2n+1,\tau_2} \rangle \\ &\quad \langle \sigma_{2n-1,\tau_2} \sigma_{2n-1,\tau_2} | e^{-\beta h_{2n-1,2n}/M} | \sigma_{2n,\tau_2} \sigma_{2n,\tau_2} \rangle \\ &\quad \cdots \\ &\quad \langle \sigma_{2n,\tau_M} \sigma_{2n,\tau_1} | e^{-\beta h_{2n,2n+1}/M} | \sigma_{2n+1,\tau_M} \sigma_{2n+1,\tau_1} \rangle. \end{aligned} \quad (11)$$

This quantum transfer matrix is graphically shown in Fig. 4. Here M is the Trotter number and τ_i is the discretized imaginary time whose intervals $\tau_{i+1} - \tau_i = \beta_0 = \beta/M$. In Eq. (11) σ_{2n,τ_i} represents states of the site $2n$ corresponding to a given imaginary time τ_i . The Hamiltonian H is assumed to be decomposed into two parts $H_{\text{odd}} = \sum_{n=1}^{L/2} h_{2n-1,2n}$ and $H_{\text{even}} = \sum_{n=1}^{L/2} h_{2n,2n+1}$ so that we can evaluate the matrix element of the exponential function. Since the partition function Z is given by the trace of the product of the quantum transfer matrix

$$\begin{aligned} Z &= \text{Tr } e^{-\beta H} \\ &= \lim_{M \rightarrow \infty} \text{Tr} (e^{-\beta H_{\text{odd}}/M} e^{-\beta H_{\text{even}}/M})^M \\ &= \lim_{M \rightarrow \infty} \text{Tr} \left[\prod_{n=1}^{N/2} (e^{-\beta h_{2n-1,2n}/M}) \prod_{n=1}^{N/2} (e^{-\beta h_{2n,2n+1}/M}) \right]^M \\ &= \lim_{M \rightarrow \infty} \text{Tr} \left[\prod_{n=1}^{L/2} \mathcal{T}_n(M) \right], \end{aligned} \quad (12)$$

thermodynamic properties of $L \rightarrow \infty$ are determined by the maximum eigenvalue and its eigenvectors. To obtain the eigenvalue and the eigenvectors for a large Trotter number M , we iteratively increase the size of the quantum transfer matrix using a similar algorithm to the zero-temperature DMRG.

We first represent the quantum transfer matrix as

$$\mathcal{T}_{(M)} = \begin{cases} \mathcal{T}_{(M)}^A \mathcal{T}_{(M)}^B, & \text{for } M : \text{even} \\ \mathcal{T}_{(M)}^{A'} \mathcal{T}_{(M)}^{B'}, & \text{for } M : \text{odd} \end{cases} \quad (13)$$

Thus the transfer matrix for $M = 2$ is

$$\begin{aligned} &\mathcal{T}_{(M=2)}(\sigma_{2n-1,\tau_1} \sigma_{2n-1,\tau_1} \sigma_{2n-1,\tau_2} \sigma_{2n-1,\tau_2}; \\ &\quad \sigma_{2n+1,\tau_1} \sigma_{2n+1,\tau_1} \sigma_{2n+1,\tau_2} \sigma_{2n+1,\tau_2}) \\ &= \sum_{\sigma_{2n,\tau_1}} \sum_{\sigma_{2n,\tau_2}} \\ &\quad \mathcal{T}_{(M=2)}^A(\sigma_{2n-1,\tau_1} \sigma_{2n-1,\tau_1} \sigma_{2n,\tau_2}; \sigma_{2n,\tau_1} \sigma_{2n+1,\tau_1} \sigma_{2n+1,\tau_2}) \\ &\quad \mathcal{T}_{(M=2)}^B(\sigma_{2n-1,\tau_2} \sigma_{2n-1,\tau_2} \sigma_{2n,\tau_1}; \sigma_{2n,\tau_2} \sigma_{2n+1,\tau_2} \sigma_{2n+1,\tau_1}). \end{aligned} \quad (14)$$

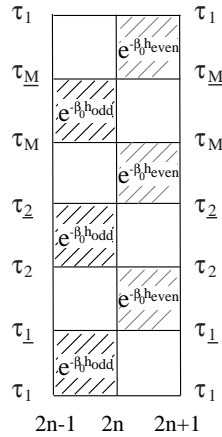


FIG. 4. The quantum transfer matrix for $M = 3$. The h_{odd} and h_{even} represent $h_{2n-1,2n}$ and $h_{2n,2n+1}$, respectively. $\Delta\tau = \tau_{i+1} - \tau_i = \beta_0$ and $\beta = M\beta_0$.

Here we have introduced $\mathcal{T}_{(M=2)}^A$ and $\mathcal{T}_{(M=2)}^B$ which are defined as

$$\begin{aligned} & \mathcal{T}_{(M=2)}^A(\sigma_{2n-1,\tau_1}\sigma_{2n-1,\tau_1}\sigma_{2n,\tau_2}; \sigma_{2n,\tau_1}\sigma_{2n+1,\tau_1}\sigma_{2n+1,\tau_2}) \\ &= \sum_{\sigma_{2n}, \tau_1} \langle \sigma_{2n-1,\tau_1}\sigma_{2n-1,\tau_1} | e^{-\beta h_{\text{odd}}/M} | \sigma_{2n,\tau_1}\sigma_{2n,\tau_1} \rangle \\ & \quad \langle \sigma_{2n,\tau_1}\sigma_{2n,\tau_2} | e^{-\beta h_{\text{even}}/M} | \sigma_{2n+1,\tau_1}\sigma_{2n+1,\tau_2} \rangle, \end{aligned} \quad (15)$$

$$\begin{aligned} & \mathcal{T}_{(M=2)}^B(\sigma_{2n-1,\tau_2}\sigma_{2n-1,\tau_2}\sigma_{2n,\tau_1}; \sigma_{2n,\tau_2}\sigma_{2n+1,\tau_2}\sigma_{2n+1,\tau_1}) \\ &= \sum_{\sigma_{2n}, \tau_2} \langle \sigma_{2n-1,\tau_2}\sigma_{2n-1,\tau_2} | e^{-\beta h_{\text{odd}}/M} | \sigma_{2n,\tau_2}\sigma_{2n,\tau_2} \rangle \\ & \quad \langle \sigma_{2n,\tau_2}\sigma_{2n,\tau_1} | e^{-\beta h_{\text{even}}/M} | \sigma_{2n+1,\tau_2}\sigma_{2n+1,\tau_1} \rangle. \end{aligned} \quad (16)$$

where $h_{\text{odd}} = h_{2n-1,2n}$ and $h_{\text{even}} = h_{2n,2n+1}$. Then we iteratively increase M of $\mathcal{T}_{(M)}^A$ and $\mathcal{T}_{(M)}^B$ as

$$\mathcal{T}_{(M)}^A e^{-\beta_0 h_{\text{odd}}} \rightarrow \mathcal{T}_{(M+1)}^{A'} \quad (17)$$

$$e^{-\beta_0 h_{\text{even}}} \mathcal{T}_{(M)}^B \rightarrow \mathcal{T}_{(M+1)}^{B'}, \quad (18)$$

$$\mathcal{T}_{(M)}^{A'} e^{-\beta_0 h_{\text{even}}} \rightarrow \mathcal{T}_{(M+1)}^A \quad (19)$$

$$e^{-\beta_0 h_{\text{odd}}} \mathcal{T}_{(M)}^{B'} \rightarrow \mathcal{T}_{(M+1)}^B. \quad (20)$$

The example for the increase of M , Eqs. (17) and (18), for $M = 2$ is graphically shown in Fig. 5.

In order to represent the transfer matrix in a restricted number of basis states, we have to select important basis states which have significant weight for the representation of the transfer matrix. For this purpose we use the generalized asymmetric density matrix similar to that used in the zero-temperature DMRG. For example, the density matrix which we use in the procedure Eq. (17) for $M = 2$ is

$$\begin{aligned} & \rho(\sigma_{2n-1,\tau_1}\sigma_{2n-1,\tau_2}; \sigma_{2n+1,\tau_1}\sigma_{2n+1,\tau_2}) \\ &= \sum_{\sigma_{\tau_1}} \sum_{\sigma_{\tau_2}} V^L(\sigma_{\tau_1}\sigma_{2n-1,\tau_1}, \sigma_{2n-1,\tau_2}\sigma_{\tau_2}) \\ & \quad V^R i\sigma_{\tau_1}\sigma_{2n+1,\tau_1}, \sigma_{2n+1,\tau_2}\sigma_{\tau_2}) \end{aligned} \quad (21)$$

where V^L and V^R are the left and right eigenvectors of $\mathcal{T}_{(M=2)}$ which have the maximum eigenvalue. The V^L and V^R are generally different owing to the non-Hermite property of the transfer matrix. The diagonalization of the density matrix provides eigenvectors, v_α^L and v_α^R , which satisfies the equations

$$\sum_{\sigma_{\tau_1}\sigma_{\tau_2}} v_\alpha^L(\sigma_{\tau_1}\sigma_{\tau_2})\rho(\sigma_{\tau_1}\sigma_{\tau_2}; \sigma'_{\tau_1}\sigma'_{\tau_2}) = \gamma_\alpha v_\alpha^L(\sigma'_{\tau_1}\sigma'_{\tau_2}) \quad (22)$$

$$\sum_{\sigma_{\tau_1}\sigma_{\tau_2}} \rho(\sigma'_{\tau_1}\sigma'_{\tau_2}; \sigma_{\tau_1}\sigma_{\tau_2})v_\alpha^R(\sigma_{\tau_1}\sigma_{\tau_2}) = \gamma_\alpha v_\alpha^R(\sigma'_{\tau_1}\sigma'_{\tau_2}). \quad (23)$$

We select the m eigenvectors which have the largest eigenvalues γ_α , and we use them as the new basis states

$$\langle \alpha_{2n-1} | = \sum_{\sigma_{2n-1}, \tau_1} \sum_{\sigma_{2n-1}, \tau_2} v_\alpha^L(\sigma_{2n-1,\tau_1}\sigma_{2n-1,\tau_2}) \langle \sigma_{2n-1,\tau_1}\sigma_{2n-1,\tau_2} |, \quad (24)$$

$$| \alpha_{2n+1} \rangle = \sum_{\sigma_{2n+1}, \tau_1} \sum_{\sigma_{2n+1}, \tau_2} v_\alpha^R(\sigma_{2n+1,\tau_1}\sigma_{2n+1,\tau_2}) | \sigma_{2n+1,\tau_1}\sigma_{2n+1,\tau_2} \rangle. \quad (25)$$

Then we represent $\mathcal{T}_{(M=3)}^{A'}$ as

$$\begin{aligned} & \mathcal{T}_{(M=3)}^{A'}(\sigma_{2n-1,\tau_1}\alpha_{2n-1,\tau_1}\sigma_{2n-1,\tau_2}; \sigma_{2n,\tau_1}\alpha'_{2n+1,\tau_1}\sigma_{2n,\tau_2}) \\ &= \sum_{\sigma_{2n-1}, \tau_1} \sum_{\sigma_{2n-1}, \tau_2} \sum_{\sigma_{2n+1}, \tau_1} \sum_{\sigma_{2n+1}, \tau_2} \sum_{\sigma_{2n}, \tau_1} v_\alpha^R(\sigma_{2n-1,\tau_1}\sigma_{2n-1,\tau_2})v_{\alpha'}^L(\sigma_{2n+1,\tau_1}\sigma_{2n+1,\tau_2}) \\ & \quad \mathcal{T}_{(M=2)}^A(\sigma_{2n-1,\tau_1}\sigma_{2n-1,\tau_1}\sigma_{2n,\tau_2}; \sigma_{2n,\tau_1}\sigma_{2n+1,\tau_1}\sigma_{2n+1,\tau_2}) \\ & \quad \langle \sigma_{2n-1,\tau_2}\sigma_{2n-1,\tau_2} | e^{-\beta h_{\text{odd}}/M} | \sigma_{2n,\tau_2}\sigma_{2n,\tau_2} \rangle. \end{aligned} \quad (26)$$

We repeat similar procedure for Eqs. (17) to (26) and obtain the maximum eigenvalue and its eigenvectors of the quantum transfer matrix for a desired M .

Compared with the zero-temperature DMRG algorithm the finite- T DMRG is more subtle from the point of view of numerical stability. The asymmetric density matrix sometimes yields complex eigenvalues, although in principle they must be real. To avoid those unphysical complex eigenvalues we need accurate numerical calculations taking account of various symmetries of the system.

The free energy per site of the infinite system is obtained from the maximum eigenvalue λ of the transfer matrix as $F = -(T/2) \ln \lambda$. Static quantities like specific heat and susceptibilities are obtained from the free energy. The specific heat is calculated by the numerical derivatives of F with respect to the temperature T .

The spin and charge susceptibilities are calculated by a shift of F under an applied magnetic field or chemical potential.

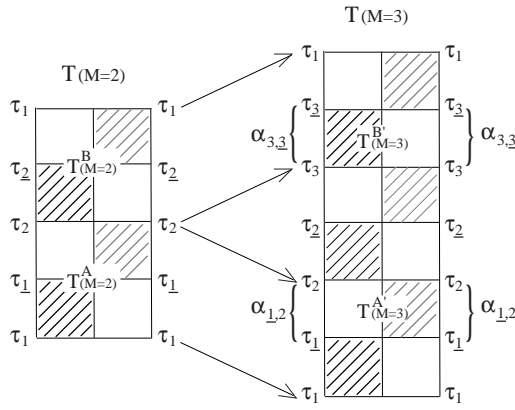


FIG. 5. Increasing of M of the quantum transfer matrix \mathcal{T} . The $\alpha_{n,m}$ is the indices of the new basis states.

The calculation of the dynamic quantities requires additional steps. We first calculate correlation functions in the β direction. This calculation requires good accuracy for the eigenvectors of the transfer matrix $\langle \Psi^L |$ and $|\Psi^R \rangle$. Thus it is necessary to use the finite system algorithm of the DMRG. The Green's function in the β direction is obtained from the left and the right eigenvectors of the transfer matrix whose eigenvalue is the largest (See Fig. 6):

$$G(\tau_j) \equiv -\text{Tr}\{e^{-\beta H} c_{i\sigma}(\tau_j) c_{i\sigma}^\dagger(0)\}/Z = -\langle \Psi^L | c_{i\sigma}(\tau_j) c_{i\sigma}^\dagger(0) | \Psi^R \rangle. \quad (27)$$

Similarly a local dynamic correlation function $\chi_{AB}(\tau_j)$ is obtained as

$$\chi_{AB}(\tau_j) \equiv \text{Tr}\{e^{-\beta H} A_i(\tau_j) B_i(0)\}/Z = \langle \Psi^L | A_i(\tau_j) B_i(0) | \Psi^R \rangle. \quad (28)$$

By Fourier transformation, the Green's function and the the dynamic correlation function as functions of the imaginary frequencies are obtained as

$$G(i\omega_n) = \frac{\beta}{M} \sum_j e^{i\omega_n \tau_j} G(\tau_j), \quad (29)$$

$$\chi_{AB}(i\omega_n) = \frac{\beta}{M} \sum_j e^{i\omega_n \tau_j} \chi_{AB}(\tau_j), \quad (30)$$

where ω_n is the Matsubara frequency that is $\pi(2n+1)/\beta$ for fermionic operators and $2\pi n/\beta$ for bosonic operators.

The real frequency Green's function and dynamic susceptibility are obtained by the analytic continuation to the real frequency axis. We can use the Padé approximations or the maximum entropy method for this purpose. The former method is based on the fittings of

$G(i\omega_n)$ or $\chi_{AB}(i\omega_n)$ by rational functions of frequency $i\omega_n$ which are analytically continued to the real axis by $i\omega_n \rightarrow \omega + i\delta$.

The maximum entropy method is based on the spectral representations

$$G(\tau) = \int_{-\infty}^{\infty} \rho(\omega) \frac{e^{-\tau\omega}}{1 + e^{-\beta\omega}} d\omega, \quad (31)$$

$$\chi_{AB}(\tau) = \int_{-\infty}^{\infty} \frac{1}{\pi} \text{Im} \chi_{AB}(\omega) \frac{e^{-\tau\omega}}{1 - e^{-\beta\omega}} d\omega, \quad (32)$$

with $\rho(\omega) = -\frac{\text{Im}}{\pi} G(\omega + i\delta)$ being the density of state. Starting from a flat spectrum, this method finally finds optimal $\rho(\omega)$ and $\chi_{AB}(\omega)$ that reproduce $G(\tau)$ and $\chi_{AB}(\tau)$ best.

The dynamical structure factor $S_{AB}(\omega)$ is related to the imaginary part of $\chi_{AB}(\omega)$ through the fluctuation dissipation theorem,

$$\text{Im} \chi_{AB}(\omega) = \pi(1 - e^{-\beta\omega}) S_{AB}(\omega). \quad (33)$$

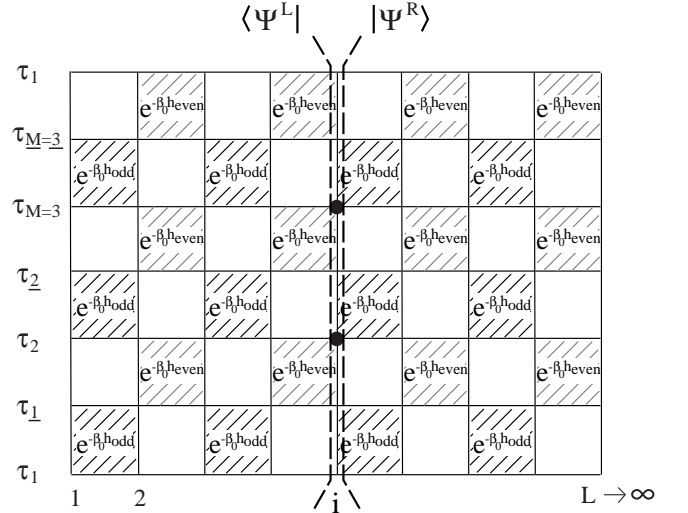


FIG. 6. Schematic diagram of the calculation of the imaginary time correlation function $\langle \Psi^L | c_{i\sigma}(\tau_3) c_{i\sigma}^\dagger(\tau_2) | \Psi^R \rangle$. The Trotter number of this example is $M = 3$.

In section III we use the standard zero-temperature DMRG method to study the ground-state properties of the paramagnetic metallic phase. In section IV after a brief discussion of the ground-state properties by using the zero-temperature DMRG, finite temperature properties of the Kondo spin liquid phase will be discussed extensively by using the finite- T DMRG.

III. TOMONAGA-LUTTINGER LIQUID PROPERTIES OF THE PARAMAGNETIC METALLIC PHASE

This section concerns with the paramagnetic phase away from half-filling, see Fig.1. Since there is no symme-

try breaking it is natural to consider that away from half-filling the translationally invariant Kondo lattice model is metallic. In one dimension it is well known that various interacting metallic systems including the Hubbard model and the t - J model belong to the universality class of Tomonaga-Luttinger liquids [11]. Therefore, the first question concerning the paramagnetic metallic phase of the Kondo lattice model is whether it belongs to this class or not.

The spin-1/2 Tomonaga-Luttinger liquids have gapless charge and spin excitations. In one dimension the charge excitations are characterized by the velocity of the charge density v_ρ and the correlation exponent K_ρ . Similarly, the spin excitations are characterized by the velocity of the spin density v_σ , but the correlation exponent in the spin sector is fixed by the SU(2) symmetry, $K_\sigma = 1$. The low-energy physics of a Tomonaga-Luttinger liquid is completely determined when these parameters are obtained. For example, the spin and charge susceptibilities are given by

$$\chi_\sigma = \frac{2}{\pi v_\sigma}, \quad (34)$$

$$\chi_\rho = \frac{2K_\rho}{\pi v_\rho}, \quad (35)$$

Reflecting the gapless excitations, the density-density and spin-spin correlation functions show power-law decays where the exponents are determined by the correlation exponent, K_ρ . The asymptotic forms of the density-density and spin-spin correlation functions are

$$\langle n(x)n(0) \rangle = K_\rho/(\pi x)^2 + A_1 \cos(2k_F x)x^{-(1+K_\rho)} + A_2 \cos(4k_F x)x^{-4K_\rho}, \quad (36)$$

$$\langle S(x) \cdot S(0) \rangle = 1/(\pi x)^2 + B_1 \cos(2k_F x)x^{-(1+K_\rho)}, \quad (37)$$

where $k_F = \pi\rho/2$, with ρ being the density of charge carriers, is the Fermi momentum. The logarithmic corrections are neglected in Eqs.(36) and (37) [12].

For the Hubbard model or the t - J model, the definition of the density of carriers is straightforward. On the other hand, for the Kondo lattice model it is already questionable. When we take naively the conduction electrons as carriers, then the Fermi momentum is given by $k_F = k_{Fs} = \pi n_c/2$. However, a different point of view is possible. Let us consider the Kondo lattice model as an effective Hamiltonian for the periodic Anderson model. For the latter, the density of carriers is the sum of the f electron density and the conduction electron density. According to the Luttinger sum rule [1] the position of Fermi points do not change when the interaction is increased as long as the ground state remains paramagnetic. Therefore this property may be carried over to the Kondo lattice model and it would be also natural to assume $k_F = k_{Fl} = \pi(1 + n_c)/2$ for the Kondo lattice model.

Concerning the paramagnetic metallic phase, there are two basic questions:

- (1) Is it a Tomonaga-Luttinger liquid?
- (2) If it is the case, what is the size of the Fermi momentum? Is it large, $k_{Fl} = \pi(1 + n_c)/2$ or small, $k_{Fs} = \pi n_c/2$? The DMRG is a powerful method to address these questions.

Let us define the ground-state energy in a given spin- S subspace for a finite system with L -sites by $E_g(L, N_c, S)$ where N_c is the number of conduction electrons. In the following we will consider only even L and N_c and thereby integer S . The spin gap of a finite system is defined by

$$\Delta_s(L) = E_g(L, N_c, S=1) - E_g(L, N_c, S=0). \quad (38)$$

Concerning the charge excitations we study the difference of the chemical potentials, $\mu_+ - \mu_-$ which is given by

$$2\mu_+ = E_g(L, N_c + 2, S=0) - E_g(L, N_c, S=0), \quad (39)$$

$$2\mu_- = E_g(L, N_c - 2, S=0) - E_g(L, N_c, S=0). \quad (40)$$

Figure 7 shows (a) the spin excitation gap and (b) the difference of the chemical potentials as a function of inverse of the system size. For the example the density of conduction electrons are fixed to $n_c = 2/3$ [13]. Both quantities go to zero as $1/L \rightarrow 0$, which means that the spin excitations and the charge excitations are gapless. Therefore it is most likely that the paramagnetic metallic phase of the Kondo lattice model belongs to the universality class of the Tomonaga-Luttinger liquids.

Now we will determine the parameters of the Tomonaga-Luttinger liquid. From the slope of the spin gap the velocity of the spin excitations are determined by

$$\Delta_s(L) = v_\sigma \pi/L, \quad (41)$$

since the lowest spin excitation of a finite system with the open boundary condition has the momentum π/L . The difference of the chemical potentials is related with the charge susceptibility by

$$\mu_+ - \mu_- = \frac{2}{\chi_\rho L}. \quad (42)$$

The values in Table I for v_σ and χ_ρ are determined from the slopes. The values of the spin susceptibility in the Table I is obtained from the spin velocity through Eq.(34).

To determine the charge velocity and the correlation exponent separately, another independent measurement is necessary. The correlation exponent K_ρ may be determined from the density-density or the spin-spin correlation functions. However, determination of the exponent of a power law decay is the most difficult for any numerical calculations. In order to determine K_ρ we need to see the long-range behaviors of the correlation functions with sufficient accuracy. Instead of looking at the correlation functions we looked at the Friedel oscillations because the latter are numerically more reliable than the former [13,14]. The reason for this is that the correlation functions are site off-diagonal, while the Friedel oscillations are site diagonal.

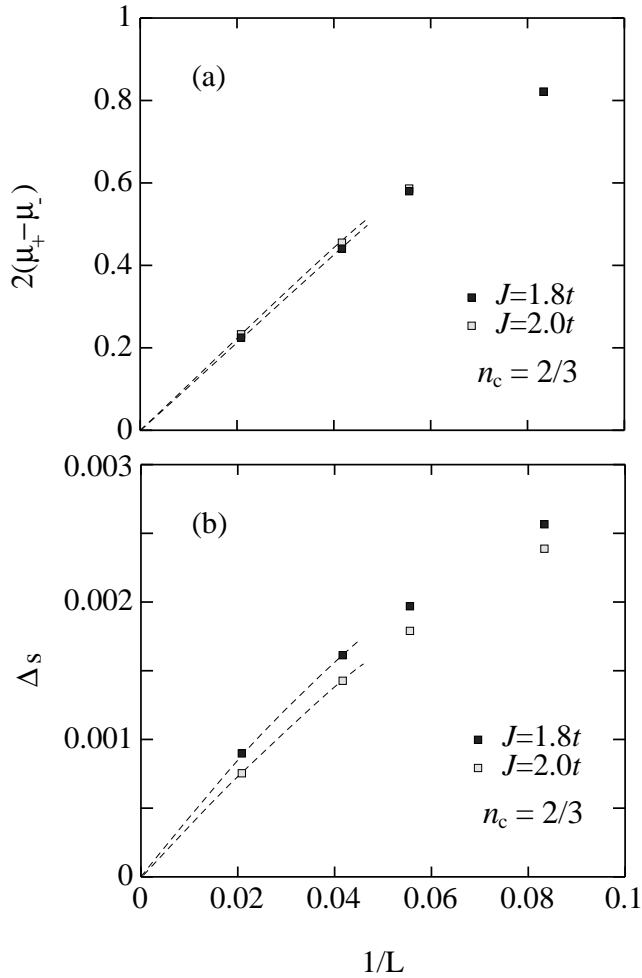


FIG. 7. (a) Size dependence of the difference of the chemical potentials, $\mu_+ - \mu_-$, in the one dimensional Kondo lattice model. (b) Size dependence of the spin gap. L is the system size and the density of conduction electrons is fixed to $n_c = 2/3$. The energy unit is t . Typical truncation errors in the DMRG calculations are 10^{-4} .

TABLE I. Luttinger liquid parameters of the one dimensional Kondo lattice model. The carrier density n_c is $2/3$. The energy unit is t . The errors are estimated from the ambiguity of the power law decay of the charge density Friedel oscillations.

	K_ρ	v_σ	χ_σ	v_ρ	χ_ρ
$J/t = 0$	1	-	-	1.73	0.37
$J/t = 1.5$	0.19 ± 0.03			0.30 ± 0.06	0.42
$J/t = 1.8$	0.24 ± 0.02	0.014	46	0.41 ± 0.06	0.38
$J/t = 2.0$	0.27 ± 0.02	0.011	56	0.48 ± 0.06	0.36

The Friedel oscillations are density oscillations induced by a local perturbation. In a Tomonaga-Luttinger liquid, power law anomalies in correlation functions naturally reflect themselves in the Friedel oscillations. The usual Friedel oscillations induced by an impurity potential are given by

$$\delta\rho(x) \sim C_1 \cos(2k_F x) x^{(-1-K_\rho)/2} + C_2 \cos(4k_F x) x^{-2K_\rho} \quad (43)$$

as a function of the distance x from the impurity [15–17]. Analogously, spin density oscillations induced by a local magnetic field behave as

$$\sigma(x) \sim D_1 \cos(2k_F x) x^{-K_\rho}. \quad (44)$$

Thus, we can determine K_ρ from the asymptotic form of the oscillations. It is worth to be noted that origin of the RKKY interaction may be traced back to the spin density oscillations induced by a localized spin.

The charge density oscillations induced by the open boundary conditions are shown in Fig.8 for $J = 1.5t$ and $J = 2.5t$ at the density $n_c = 4/5$ [14]. The spin density oscillations induced by the local magnetic fields applied at the both ends with opposite directions are shown in Fig.9 for the same set of parameters [14]. It is clearly seen that the dominant period of the charge density oscillations is five sites, $q = 2\pi/5$, while for the spin density oscillations ten sites, $q = \pi/5$.

In the strong coupling limit of the Kondo lattice model, each conduction electron form a local singlet with the f spin on the same site. However away from half-filling these singlets can move in the lattice with the effective hopping matrix elements reduced by half. Equivalently, we can regard the unpaired f spins as mobile objects with the reduced hopping energy $t/2$ with its sign reversed. Note that in the original model hopping matrix elements are defined by $-t$. Thus the effective model of the strong coupling limit is the t -model where the number of carriers is $L - N_c$ and double occupancy of the carriers is prohibited.

The charge response of the system is identical to the spinless Fermions where the Fermi point is given by $\pi - \pi(1 - n_c) = \pi n_c$. Therefore the induced charge density shows oscillations corresponding to $2\pi n_c$ which is equivalent to $4k_F s$ and $4k_F l$. This analysis shows that in the strong coupling limit the amplitude of the $4k_F$ oscillations dominates over the $2k_F$ oscillations for the charge Friedel oscillations, Eq.(43). The period of five sites is naturally understood in this way and we have confirmed that for a weaker coupling the amplitude of the $2k_F$ oscillation develops.

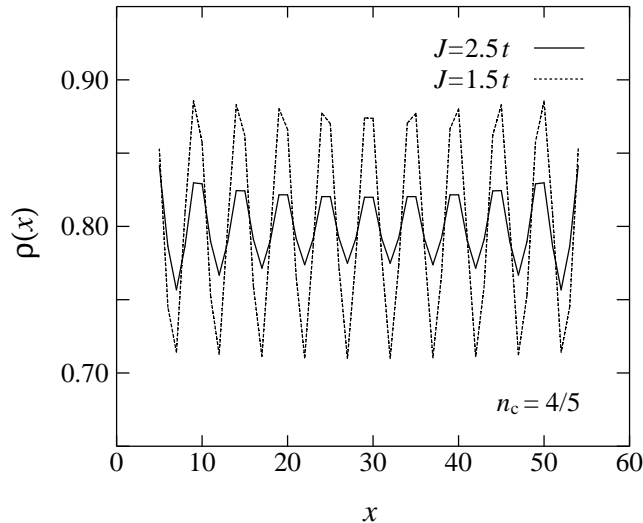


FIG. 8. Charge density oscillations of the Kondo lattice model. The system size is 60 sites and the carrier density is $n_c = 4/5$. The solid line and the broken line correspond to $J = 2.5t$ and $J = 1.5t$, respectively. Typical truncation errors in the DMRG calculations are 1×10^{-6} for $J = 2.5t$ and 3×10^{-6} for $J = 1.5t$.

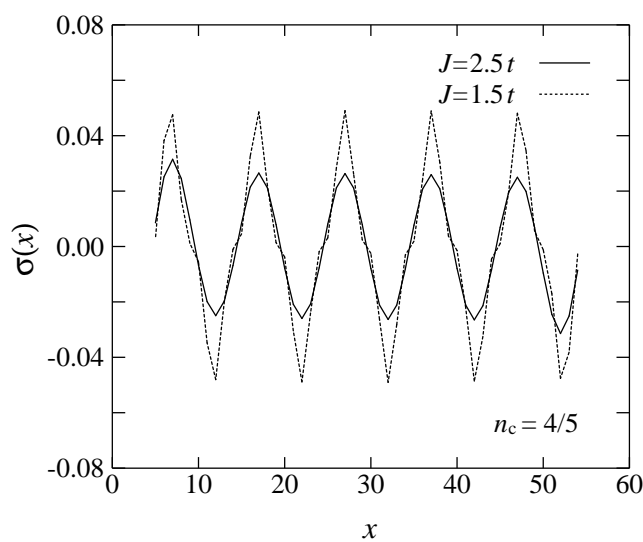


FIG. 9. Spin density oscillations of the Kondo lattice model. The system size is 60 sites and the carrier density is $n_c = 4/5$. The solid line and the broken line correspond to $J = 2.5t$ and $J = 1.5t$, respectively. The strength of the local magnetic field h is $0.1t$. Typical truncation errors in the DMRG calculations are 1×10^{-6} for $J = 2.5t$ and 3×10^{-6} for $J = 1.5t$.

When we consider the spins of the unpaired f electrons, there remains a macroscopic 2^{L-N_c} -fold degeneracy. Concerning the spin sector the lifting of the degeneracy is essential. For the specific model where the degeneracy is lifted by the next nearest neighbor hoppings it is shown analytically that the Fermi surface is big, $k_F = k_{FL}$ [18]. For a finite J the degeneracy of the Kondo lattice model is always lifted. The period of

ten sites of the spin density Friedel oscillations shown in Fig. 9 indicate that the $2k_F$ oscillations corresponding to $2k_{FL}$ are actually observed. Figure 10 show that the $2k_{FL}$ oscillations corresponding to the large Fermi surface are always dominating in the paramagnetic phase for various coupling constants and various densities.

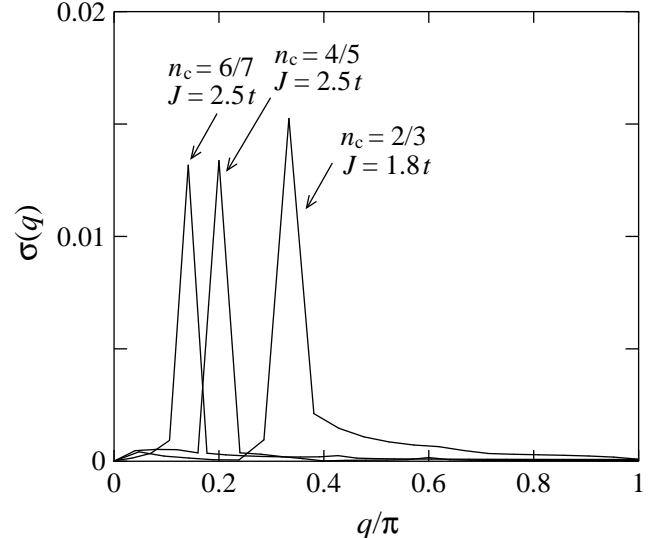


FIG. 10. Fourier components of the spin density Friedel oscillations.

The Friedel oscillations obtained by the DMRG method clearly indicate that the Fermi surface of the Kondo lattice model is large. At the early stage, the conclusions of the bosonization studies were controversial. In the area of the paramagnetic metallic phase Fujimoto and Kawakami obtained the Tomonaga-Luttinger liquid with a large Fermi surface, while White and Affleck predicted a Luther-Emery liquid with a spin gap [19,20]. Later, it was argued that an additional direct Heisenberg coupling between the f -spins is necessary to stabilize the Luther-Emery liquid [21]. Furthermore, the existence of a gapless excitation with the momentum of $2k_{FL}$ is shown rigorously by the Lieb-Schultz-Mattis construction [22].

In order to obtain the correlation exponent K_ρ , we used the slope of the envelope function of the charge density oscillations, assuming that dominant component of the oscillations is the $4k_F$ oscillations. Figure 11 shows K_ρ thus determined for the exchange coupling constants from $J = 4.0t$ to $1.5t$. The density of conduction electrons is fixed to $n_c = 2/3$. K_ρ is always smaller than $1/2$ and monotonically decreases with decreasing J . The limiting value of $K_\rho = 1/2$ in the strong coupling limit is easy to understand since the strong coupling limit of the Kondo lattice model is equivalent to the $U = \infty$ Hubbard model.

The correlation exponent shows a small discontinuity at the boundary between the ferromagnetic and paramagnetic phases, $J_c = 2.4t$ for $n_c = 2/3$. Below J_c , the K_ρ decreases faster and becomes lower than $1/3$, which means that the long range behavior of the density-density correlation is governed by the $4k_F$ oscillations rather than

the $2k_F$ oscillations. With further decreasing J , the K_ρ seems to cross the value $3 - 2\sqrt{2} \sim 0.17$. Since the exponent of the power law anomaly of the momentum distribution function is given by $(K_\rho + 1/K_\rho - 2)/4$, the power law anomaly is removed below this point and a clear Fermi surface can not be seen anymore.

Through the study of the Friedel oscillations by the DMRG method, it has become clear that the paramagnetic metallic phase of the one dimensional Kondo lattice model is a Tomonaga-Luttinger liquid with a large Fermi surface. This Tomonaga-Luttinger liquid is unique in the sense that the K_ρ is smaller than $1/2$. The small K_ρ may be attributed to the long range nature of effective interactions with strong retardation [12,23]. Recently, observation of the Friedel oscillations by the DMRG method is shown to be useful also for discussions of critical behaviors of the Hubbard model [24].

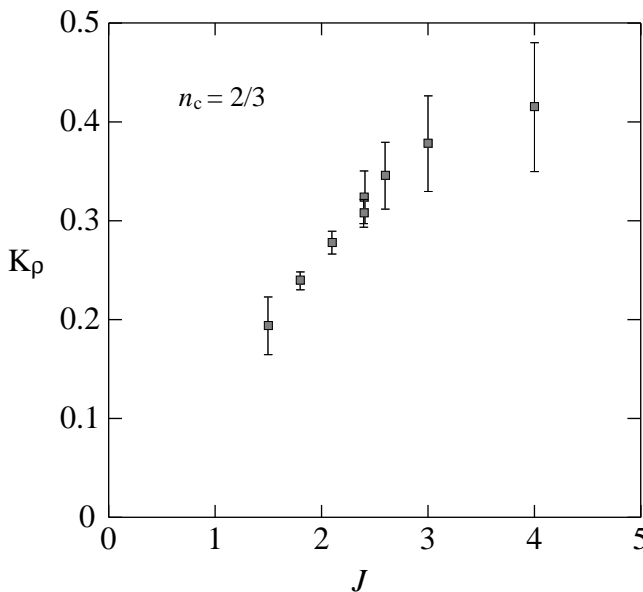


FIG. 11. Correlation exponent K_ρ estimated from the decay rate of the charge density Friedel oscillations. The errorbars are estimated from ambiguity of the power law fitting. $n_c = 2/3$. J is in units of t .

IV. KONDO SPIN LIQUID PHASE AT HALF-FILLING

The half-filled KL model is always insulating in one-dimension. This conclusion was obtained by the exact diagonalization study [5]. Based on a finite size scaling it was shown that finite excitation gap remains for any finite J . The result has been confirmed by the DMRG method [25] and later supported by the mapping to a non-linear sigma model [26] and by the bosonization approach [27]. In this section we discuss basic properties of this insulating state.

Concerning the insulating phase, the question we would like to address here is which characters distin-

guish the Kondo insulators from usual semiconductors. The most significant difference is that there are no gaps at high temperatures and they are induced as the temperature is lowered. Furthermore the excitation gaps induced by the temperature are different depending on channels. The difference of the excitation gaps and more generally the difference in the temperature dependence of various excitation spectra are naturally reflected in temperature dependence of various thermodynamic quantities.

Clearly the lowest excitation gap which is the spin gap for the Kondo insulator defines the smallest energy scale of the system. In ordinary band insulators the band gap defines the smallest energy scale which controls not only the spin excitations but also the charge excitations. It is also interesting to compare the smallest energy scale of the Kondo lattice problem with that of the single impurity Kondo effect, namely the Kondo temperature T_K . It is well known that the low temperature properties of the impurity model is governed by the single energy scale of T_K .

In the present section, first we will discuss the spin gap, the charge gap and the quasiparticle gap by the ground state DMRG. Then we will discuss temperature dependence of the spin susceptibility, the charge susceptibility and the specific heat by the finite- T DMRG. Temperature dependences of the single particle excitation spectrum, the dynamic spin-spin correlation function and the charge-charge correlation function are also discussed by the finite- T DMRG. For the analytic continuation which is necessary to discuss the dynamic quantities, it is shown that the maximum entropy method is very useful [28–30].

A. Spin, charge and quasiparticle gaps

To understand the physics of the insulating state of the half-filled Kondo lattice model, it is instructive to consider the limit of strong exchange coupling J . In this limit every f spin together with a conduction electron form a local singlet on every site. To create spin excitations the minimum energy cost is J , which is the energy difference between the local spin singlet state and the local spin triplet state. On the other hand, creation of charge excitations requires the minimum energy of $3J/2$ which corresponds to the energy cost for breaking two local singlets by transferring a conduction electron to a neighboring site.

The excitation gaps monotonically decrease with decreasing exchange constant, but they do not vanish at any finite value of J . Particularly, the weak coupling limit $J \ll t$ is interesting. In this regime the KL model is equivalent to the periodic Anderson model with strong Coulomb repulsion in the f orbitals. The salient feature of the strong Coulomb interaction in the periodic Anderson model appears in the diverging ratio between the charge and spin gaps. The limit of $J = 0$ is singular where the conduction electrons and the f spins are

decoupled, and both the spin and charge gaps vanish.

For the discussion of the gaps, we take into account also the Coulomb interaction between the conduction electrons. Since the spin and charge gaps are tiny in the weak coupling regime, it is no more justified to neglect the Coulomb interaction between the conduction electrons. This Coulomb interaction suppresses the double occupation of conduction electrons, which eventually leads to the formation of local magnetic moments of the conduction electrons. Therefore the effect of the Coulomb interaction on the spin and charge gaps of the KL model sheds lights on the nature of the gap formation in Kondo insulators.

The model we consider in this subsection is the following one-dimensional KL model with Coulomb interaction between the conduction electrons U_c :

$$H = -t \sum_{i\sigma} (c_{i\sigma}^\dagger c_{i+1\sigma} + \text{H.c.}) + J \sum_{i\mu} S_i^\mu \sigma_i^\mu + U_c \sum_i (c_{i\uparrow}^\dagger c_{i\uparrow} - \frac{1}{2})(c_{i\downarrow}^\dagger c_{i\downarrow} - \frac{1}{2}). \quad (45)$$

The Coulomb interaction is represented in the last term. In this section we consider the case of half-filling where the total number of conduction electrons is equal to the number of lattice sites L : $N_c \equiv \sum_{i\sigma} c_{i\sigma}^\dagger c_{i\sigma} = L$. This Hamiltonian is reduced to the Hubbard model in the limit of $J \rightarrow 0$, and to the usual KL model for $U_c = 0$.

In the impurity Kondo model all low temperature properties are scaled by the single energy scale $T_K \sim D \exp(-\frac{1}{\rho J})$, where ρ is the density of states of the conduction band at the Fermi level and is given by $\frac{1}{2\pi t}$ in one dimension. In contrast to the single impurity Kondo model, the KL model has many f spins which are coupled through the conduction electrons. A basic question of the lattice problem is how the intersite correlations appear in the energy scale. The simplest extension of the form of T_K may be an inclusion of an enhancement factor in the exponent: The spin gap is expected to behave as

$$\Delta_s \propto \exp\left(-\frac{1}{\alpha\rho J}\right), \quad (46)$$

where α is the enhancement factor. The Gutzwiller approximation predicts an enhancement factor $\alpha = 2$ [31]. Tsunetsugu *et al.* have estimated that the enhancement factor in one dimension is in the range of $1 \leq \alpha \leq 5/4$ by using a finite size scaling for the results obtained by the exact diagonalization [5]. In the following we present the results on the enhancement factor obtained by the DMRG.

The spin gap is obtained from the difference of the ground-state energies in the subspaces of total S^z being zero and one, Eq.(38); the SU(2) symmetry in the spin space guarantees the energy difference is the same as the spin gap in the subspace of zero total S^z . The spin gap of the bulk system is estimated from the following scaling function:

$$\Delta_s(L) = \Delta_s(\infty) + \beta L^{-2} + O(L^{-4}). \quad (47)$$

The obtained spin gaps are plotted in Fig. 12 in logarithmic scale as a function of $1/J$. The results are obtained by the extrapolation to the bulk limit using data of $L = 6, 8, 12, 18, 24, 40$. The DMRG calculations were done by using the finite system algorithm with open boundary conditions keeping up to 300 states for each block. The enhancement factor is obtained from the slope in the figure, and determined to be $\alpha = 1.4(1)$ for $U_c = 0$. There are some uncertainties in the extrapolation to the bulk limit for tiny gaps. However within the present accuracy we do not observe any indication of the logarithmic correction to the exponent which was predicted by the semiclassical approach [26].

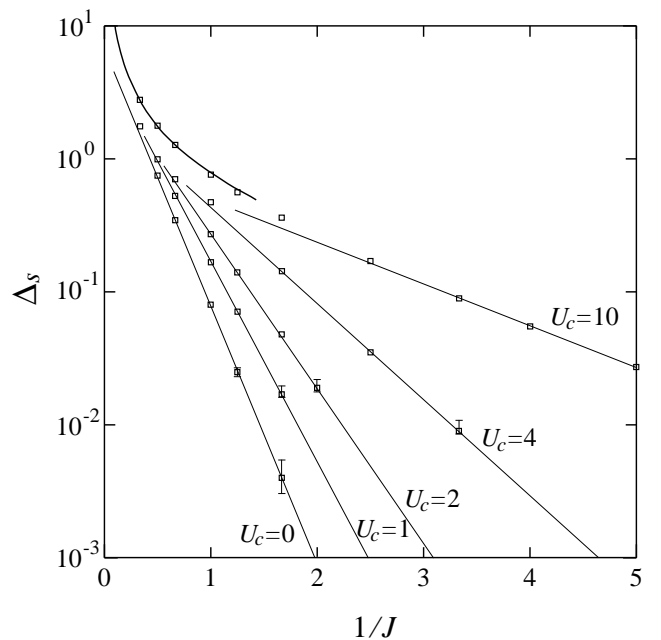


FIG. 12. Spin gap of the half-filled one-dimensional Kondo lattice model with Coulomb interaction. The thick curve represents the result of the perturbation theory in terms of t/J for $U_c = 10t$. Typical truncation error in the DMRG calculation is 10^{-6} for $J = 1$. Errorbars are estimated from L^{-1} and L^{-2} scalings. Gap energies, exchange constant J , and Coulomb interaction U_c are in units of t .

Now we consider the effect of the Coulomb interaction. In the weak coupling region it is natural to extend the form of Eq. (46) to finite U_c allowing U_c -dependence of the exponent. Indeed the numerical data are nicely fitted by this form as shown in Fig. 12. The obtained U_c -dependence is shown in Fig. 13, which indicates that $\alpha(U_c)$ increases with increasing U_c and the asymptotic behavior is linear in U_c . The KL model with the Coulomb interaction is mapped to a Heisenberg chain coupled with the localized f spins in the limit of $U_c/t \rightarrow \infty$. The linear U_c -dependence of the exponent $\alpha = 0.78U_c/t + 0.7$ in Fig. 13 means that the spin gap of the effective spin model behaves as $\Delta_s \sim \exp(-2J_{\text{eff}}/J)$ with $J_{\text{eff}} = 4t^2/U_c$.

beeing the effective coupling of the Heisenberg chain. In order to check this form we have analyzed the numerical data for the spin system obtained by Igarashi *et al.* [32], and found a good coincidence. Thus we conclude that the enhancement factor α increases monotonically with increasing U_c . This is natural since the origin of the spin gap is the singlet binding between the localized spins and the conduction electrons for which the Coulomb interaction helps by suppressing the double occupancy.

In contrast to the single impurity Kondo model, the KL model has the second energy scale that characterizes the charge excitations at low temperatures. The charge excitations keep spin quantum numbers, and the charge gap is defined by the difference of the lowest energy in the subspace of $N_c = L$ and $N_c = L + 2$: $E_g(L, N_c = L + 2, S = 0) - E_g(L, N_c = L, S = 0)$. Owing to the hidden SU(2) symmetry in the charge space, the energy difference is the same as the charge excitation gap in the subspace of the fixed number of electrons $N_c = L$ [33].

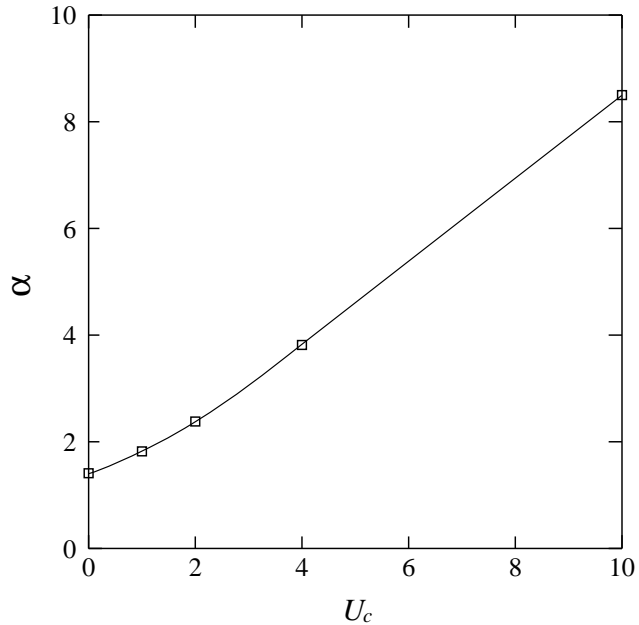


FIG. 13. U_c -dependence of the exponent of the spin gap. Coulomb interaction U_c is in units of t .

Figure 14 shows the charge gap obtained by the extrapolation to the infinite system. The results for $J = 0$ are known as the Hubbard gap of the one-dimensional Hubbard model which is exactly solved by the Bethe Ansatz [34]. The asymptotic forms of the charge gap are given by $\Delta_c \propto \sqrt{U_c t} \exp(-\frac{1}{\rho U_c})$ for small U_c , and by $\Delta_c \propto U_c - 4t$ for large U_c . The results obtained for finite J are consistent with the exact ones which are denoted by the crosses on the vertical axis.

For $U_c = 0$ the charge gap is linear in J in the small J/t limit. As is shown by the exact diagonalization study the charge gap is much bigger than the spin gap in the weak coupling regime [33]. It implies that the correlation length for the spin degrees of freedom is much longer

than the charge correlation length. Therefore for the discussion of the charge gap it is justified to assume that the spin-spin correlation length is infinitely long. Under the assumption of the infinite spin correlation length, the charge gap is calculated as

$$\Delta_c = \frac{J}{2}. \quad (48)$$

From Fig. 14 we also find that the charge gap increases with increasing Coulomb interaction U_c .

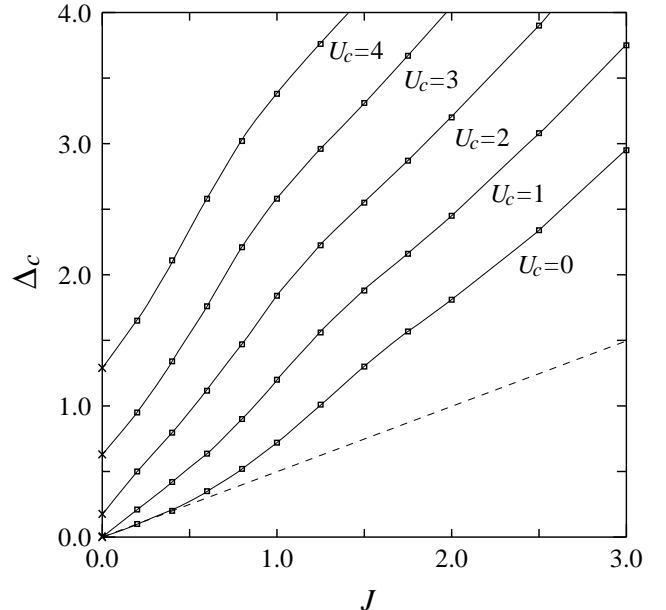


FIG. 14. Charge gap of the half-filled one-dimensional Kondo lattice model with Coulomb interaction. Results on the vertical axis are obtained from the exact solution by Lieb-Wu. Typical truncation errors in the DMRG calculation are 10^{-6} for $J = 1$ and 10^{-4} for $J = 0.2$, which are dominant source of numerical errors since the finite size scaling, Eq. (47), is well obeyed. Gap energies, exchange constant J , and Coulomb interaction U_c are in units of t .

The charge excitations are created by adding two additional electrons keeping spin quantum numbers fixed. When we put single electron in the ground state, then a quasiparticle excitation is made. Here we consider the relation between the charge gap Δ_c and the quasiparticle gap Δ_{qp} which is defined by $E_g(L, N_c = L \pm 1, S = \pm 1/2) - E_g(L, N_c = L, S = 0)$. In the strong coupling limit, $J/t \rightarrow \infty$, it is evident that the charge gap is twice the quasiparticle gap owing to the SU(2) symmetry in the charge space. In the second order perturbation in t/J , one can show that the interaction between the two additional electrons is repulsive, leading to only a phase shift. Therefore the charge gap in the bulk limit is twice the quasiparticle gap Δ_{qp} :

$$\Delta_c = 2\Delta_{qp}. \quad (49)$$

A similar argument is also valid for the periodic Anderson model [33]. Validity of this relation is checked by

the DMRG calculation in the entire region of the exchange constant J . Concerning the spin gap, the lowest spin excitation may be considered as a bound state of a quasielectron and a quasi-hole.

B. Susceptibilities at finite temperatures

The spin and charge gaps determined at zero temperature are very different in the weak coupling regime. The spin gap is exponentially small, while the charge gap is proportional to J . The large charge gap originates from the staggering internal magnetic fields induced by the long correlation length of the f spins. At finite temperatures, however, the spin correlations are subject to the thermal fluctuations. When temperature becomes comparable to the spin gap, the spin correlation length gets smaller and the whole electronic states including the charge excitation spectrum are reconstructed. In this section we study such an interplay between the spin and charge excitations at finite temperatures by looking at the thermodynamic quantities. In what follows we consider the original KL model neglecting the Coulomb interaction between the conduction electrons.

In order to calculate thermodynamic quantities we use the finite- T DMRG discussed in Sec. II [7,8]. In this method the free energy is obtained from the maximum eigenvalue of the quantum transfer matrix. The spin and charge susceptibilities are obtained from the derivatives of the free energy with respect to external magnetic field or chemical potential. The calculations are performed by the infinite system algorithm keeping 40 states per block. The truncation errors in the calculation are typically 10^{-3} and at the lowest temperature 10^{-2} for the Trotter number $M = 50$.

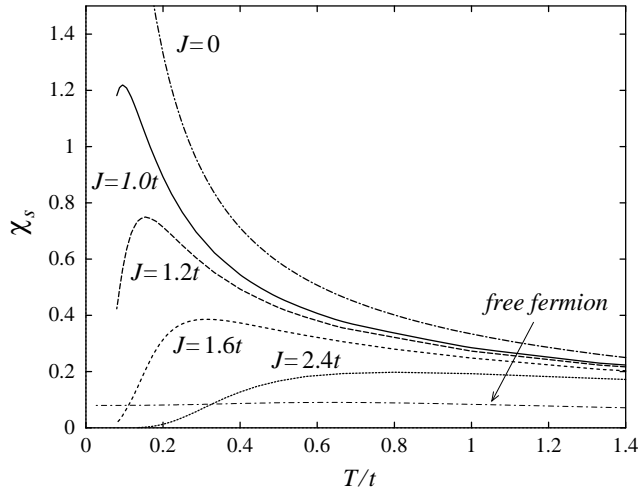


FIG. 15. Spin susceptibility of the half-filled one-dimensional Kondo lattice model. The truncation errors in the finite- T DMRG calculation are typically 10^{-3} and at the lowest temperature 10^{-2} .

We first consider the temperature dependence of the

uniform spin susceptibility. The spin susceptibility is obtained from the change of the free energy by a small magnetic field h : $\delta F = \chi_s h^2/2$. The results for $J/t = 0, 1.0, 1.2, 1.6$ and 2.4 are shown in Fig. 15.

When $J/t = 0$, the localized spins and conduction electrons are uncorrelated. The susceptibility is given by the sum of the Curie term due to the free f spins and the Pauli term of the free conduction electrons. The contribution of the Pauli susceptibility of the conduction electrons shown by the dashed line in Fig. 15 is relatively small, and the total susceptibility for $J/t = 0$ is dominated by the Curie term.

For finite J , the low temperature part of χ_s sharply drops with decreasing the temperature. This drastic change is due to the appearance of a low energy scale for the spin sector. The spin gap of $0.08t$ for $J/t = 1.0$ is consistent with the characteristic temperature at which χ_s starts to decrease deviating from the Curie law.

In order to determine the energy scale at low temperatures we estimate the activation energy by fitting the susceptibility with an exponential form. The estimated activation energy for the spin susceptibility is summarized in Table II for $J/t = 1.6, 2.4$ and 3.0 . Compared with the quasiparticle gap and the spin gap, both of which are responsible for the magnetic excitations, we conclude that the lower one of them determines the low-temperature energy scale of the spin susceptibility. This is consistent with the general form of susceptibility which is written as

$$\chi_s = Z^{-1} N^{-1} \beta \sum_m e^{-\beta E_m} \langle m | S_z^{\text{total}} | m \rangle^2, \quad (50)$$

$$Z = \sum_m e^{-\beta E_m}. \quad (51)$$

The point is that Eqs.(50) and (51) apply for both the canonical and the grand canonical ensembles by properly defining the states $|m\rangle$. In the thermodynamic limit the susceptibilities by the two ensembles should give the same answer. From this consideration it is concluded that the smaller one of the spin gap and the quasiparticle gap determines the low temperature energy scale. For the case of small exchange coupling ($J/t \ll 1$) the spin gap is smaller than the quasi-particle gap and thus the low temperature energy scale of χ_s is determined by the spin gap.

In order to see the effect of thermal fluctuations of f spins to the charge excitations, we next calculate the charge susceptibility χ_c . The χ_c is obtained from the change of the free energy due to a small shift of chemical potential μ , $\delta F = \chi_c \mu^2/2$. In the present calculation we use the fact that the chemical potential is zero at half-filling owing to the SO(4) symmetry of the model. [33] The results for $J/t = 0, 1.0, 1.2, 1.6$ and 2.4 are shown in Fig. 16.

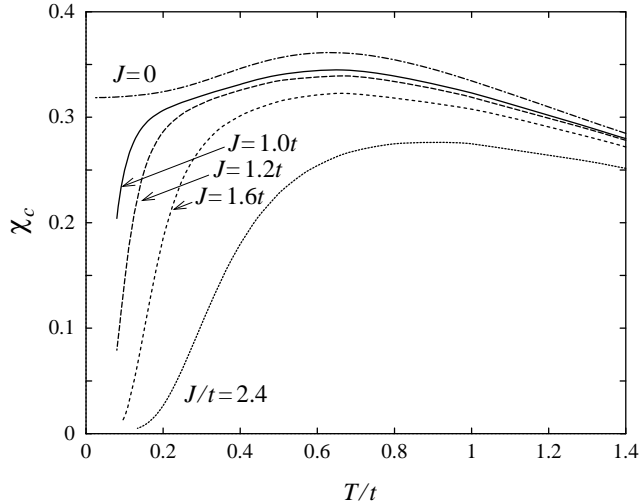


FIG. 16. Charge susceptibility of the half-filled one-dimensional Kondo lattice model.

For $J/t = 0$, χ_c does not show diverging behavior at low temperatures in contrast to χ_s . In the limit of $T = 0$, χ_c is equal to the density of state of conduction electrons which is $1/\pi t$ including the two spin directions. This is expected since the charge degrees of freedom is governed by the conduction electrons. Since there is no interaction, $\chi_c/4$ is equal to the spin susceptibility of the free conduction electrons. The slight increase in χ_c in the low-temperature region is a characteristic feature of the one-dimensional system where the density of states diverges at the band edges.

A finite value of J produces a sharp drop in χ_c at low temperatures. Similarly to χ_s , this drop is due to the appearance of low energy scale Δ_c for the charge sector. The energy scale is determined by the activation energy for the charge susceptibility. By fitting χ_c with an exponential form, the activation energy Δ_{χ_c} is obtained as listed in Table II for $J/t = 1.6, 2.4$ and 3.0 . From this table it is concluded that the quasiparticle gap determines the low-temperature energy scale of the charge susceptibility.

TABLE II. Activation energy obtained from the spin and charge susceptibilities, Δ_{χ_s} and Δ_{χ_c} , of the one-dimensional Kondo lattice model at half-filling. The quasiparticle gap Δ_{qp} and the spin gap Δ_s are obtained by the zero-temperature DMRG. The charge gap is twice the quasiparticle gap; $\Delta_c = 2\Delta_{qp}$

	Δ_{χ_s}/t	Δ_{χ_c}/t	Δ_s/t	Δ_{qp}/t
$J/t = 1.0$			0.08	0.36
$J/t = 1.2$			0.16	0.47
$J/t = 1.6$	0.45 ± 0.1	0.6 ± 0.1	0.4	0.7
$J/t = 2.4$	1.2 ± 0.1	1.0 ± 0.1	1.1	1.1
$J/t = 3.0$	1.6 ± 0.1	1.4 ± 0.1	1.8	1.5

Although the quasiparticle gap determine the exponential temperature dependence at low temperatures, it is not the single energy scale for χ_c . It may be best understood by looking at χ_c for $J/t = 1.0$. A sharp decrease of χ_c is seen at around $T \sim 0.1t$ which is much smaller than the quasiparticle gap $0.36t$ but rather close to the value of the spin gap $0.08t$. This fact suggests that the whole electronic states are reconstructed when temperature is raised up to the spin gap. We will discuss this aspect in more detail in connection with the temperature dependence of various excitation spectra.

C. Specific heat

In order to see how the entropy of the system is released, we next calculate specific heat. The specific heat is calculated from the second derivative of the free energy; $C = -T\partial^2 F/\partial T^2$. The results for $J/t = 0, 1.0, 1.2, 1.6$ and 2.4 are shown in Fig. 17.

At $J/t = 0$ the specific heat of this model is given by the sum of the delta function at $T = 0$ that originates from the free localized spins and the specific heat of free conduction electrons. For finite J they are combined to form a two-peak structure. The peak at higher temperatures is almost independent of the exchange constant and similar to the specific heat of free conduction electrons. Thus the structure at higher temperatures may be understood as the band structure effect of the one dimensional conduction electrons. In contrast to the higher temperature structure, the structure at lower temperatures strongly changes its form with J . The peak shifts towards higher temperatures and becomes broader with increasing J .

With further increasing the exchange coupling, the spin gap becomes comparable to the hopping matrix element t . In this situation various energy scales are not distinguishable and the specific heat possesses a single peak structure as shown for $J/t = 2.4$.

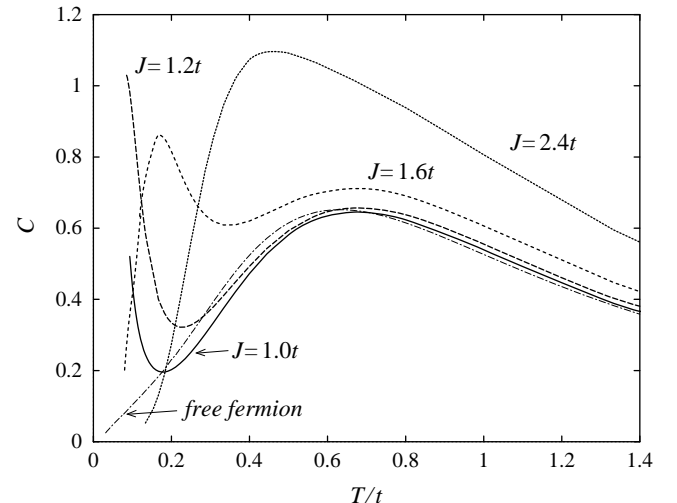


FIG. 17. Specific heat of the half-filled one-dimensional Kondo lattice model.

D. Dynamic properties

Dynamic properties of the half-filled KL model show clear features characteristic to strongly correlated insulators. Unusual temperature dependence of the excitation spectra is one of the most important features of the interacting systems. Actually the behaviors of the static susceptibilities discussed in the preceding subsection indicates that the excitation gaps develop at low temperatures.

In this section we calculate the dynamic spin and charge structure factors, $S(\omega)$ and $N(\omega)$, and the density of states, $\rho(\omega)$. By looking at their temperature dependence we can study temperature evolution of the excitation gaps and the relations among dynamic quantities. To obtain the dynamic quantities we first calculate the correlation functions in the imaginary time direction. As we have discussed in section II, the correlation functions in the imaginary time direction are directly calculated from the left and right eigenvectors obtained by applying the finite- T DMRG to the transfer matrix.

Examples of the single particle Green's function as a function of the imaginary time calculated by the finite- T DMRG are shown in Fig. 18. To obtain the spectral functions we first Fourier transform the imaginary time correlation functions and then need to perform analytic continuation from the imaginary frequency axis to the real frequency axis. One straightforward method for the analytic continuation is to use the Padé approximations. Since the DMRG calculation yields no statistical errors the Padé approximations show good convergence in many cases. However, it is still difficult to obtain the spectral functions by the Padé approximations in a stable manner when a spectrum has a nearly singular form. The reason is that the Padé approximations use rational functions of Matsubara frequencies $i\omega_n$.

Even when a spectrum has a nearly singular form, the maximum entropy method still works well. An advantage of this method is that we can explicitly use the symmetries and the positiveness of the spectral function. The results obtained by the two method are compared in Fig. 19. At high temperatures two results coincide with each other, but with decreasing the temperature the convergence of the Padé approximations becomes worse due to the growing singularity in the spectral function in the low frequency region. The results by the maximum entropy method are stable even at low temperatures. Thus in the following we employ the maximum entropy method to study temperature evolution of the dynamic correlation functions [35].

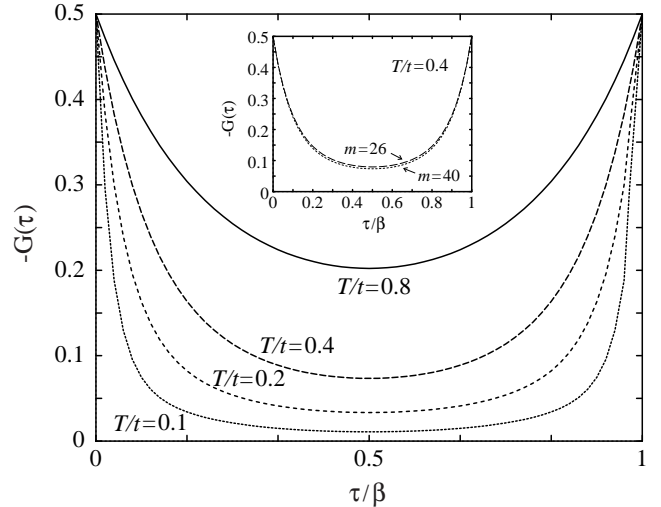


FIG. 18. Imaginary time correlation functions, $G(\tau)$, of the half-filled one-dimensional Kondo lattice model: $J/t = 1.6$. The Trotter number $M = 60$. Inset shows the results for different number of state kept m in the DMRG calculation. The truncation errors in the DMRG calculation are 2×10^{-3} for $m = 26$ and 3×10^{-4} for $m = 40$.

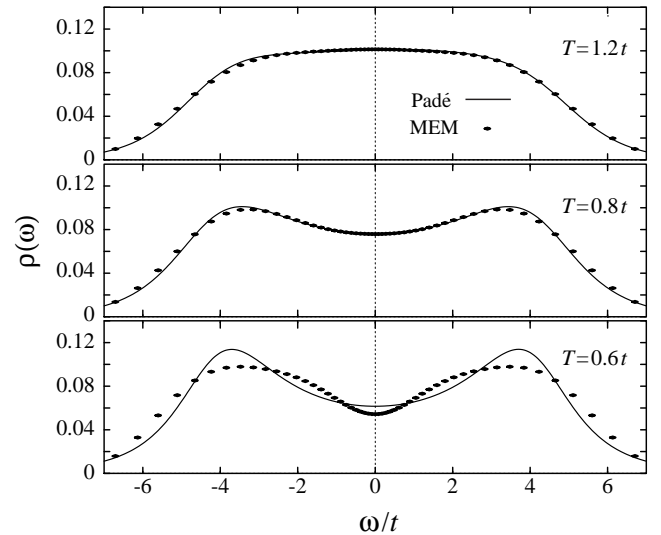


FIG. 19. Quasiparticle density of states, $\rho(\omega)$, obtained from the $G(\tau)$ by the Padé approximations and the maximum entropy method (MEM). The Trotter number $M = 60$.

The quasiparticle density of states obtained for $J/t = 1.6$ at temperatures $T/t = 0.1, 0.14, 0.2, 0.25, 0.3, 0.6$ is shown in Fig. 20. Existence of the quasiparticle gap is seen as a clear dip structure around $\omega = 0$. At low temperatures sharp peaks appear at $\omega = \pm\Delta_{qp}$ separated from the higher frequency part of the spectral weight. Sharpness of the peaks suggests the formation of the heavy quasiparticle bands at the gap edges. The high frequency part of the spectral weight extends to the region far from the edge of the free conduction band $\omega = 2t$, which shows significance of the multiple excitations accompanied with the quasiparticle excitations.

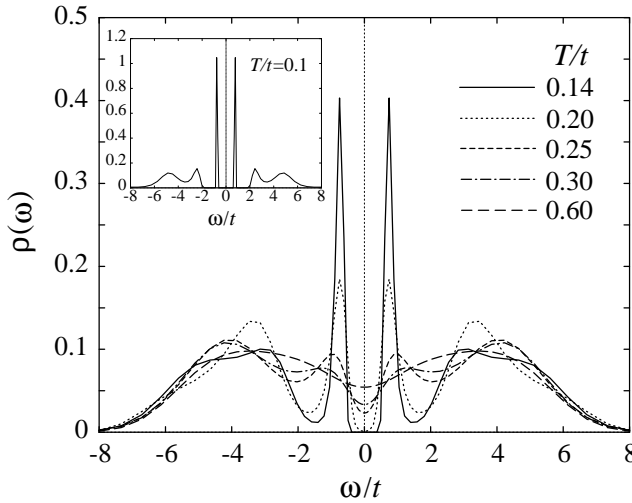


FIG. 20. Quasiparticle density of states, $\rho(\omega)$, of the half-filled one-dimensional Kondo lattice model: $J/t = 1.6$. The Trotter number $M = 60$, and the number of states kept $m = 40$.

As the temperature is increased, the peak at the threshold gets broadened and at temperatures $T \sim \Delta_s$ the peak and the accompanied dip between the low and high frequency parts completely disappear. This result shows that although the sharp peaks of the quasiparticle density of states are located at the frequency $\omega = \pm\Delta_{qp}$, it disappears around the temperature $T \sim \Delta_s$ which is much lower than $T \sim \Delta_{qp}$.

In order to see what happens at the temperatures $T \sim \Delta_s$, we next consider the f spin dynamic structure factor $S_f(\omega)$. The calculated $S_f(\omega)$ are presented in Fig. 21. At the lowest temperature the spin gap is clearly seen with a sharp peak at the gap edge. This characteristic peak has the most of the spectral weight, which shows concentrated f spin excitations at the energy scale of Δ_s . There is a broad peak in the higher frequency side. As is shown later, a similar structure and temperature dependence appear in the dynamic spin structure factor of the conduction electrons $S_c(\omega)$. Thus we conclude that through the exchange coupling excitations of the f spins are mixed with those of conduction spins, which yields this broad peak in higher frequency part of $S_f(\omega)$.

With increasing the temperature, the peak structure at $\omega = \Delta_s$ becomes broad and the spectral intensity increases around the zero frequency $|\omega| < \Delta_s$. At the temperatures $T \sim \Delta_s$, the peak position of the spectrum shifts to the zero frequency, and the peak height becomes almost temperature independent. The spectral intensity at the zero frequency is directly related to the NMR relaxation rate $1/T_1$. Hence the present results show that $1/T_1$ is nearly temperature independent at high temperatures and drastically decreases with decreasing temperature below the characteristic temperature of the order Δ_s .

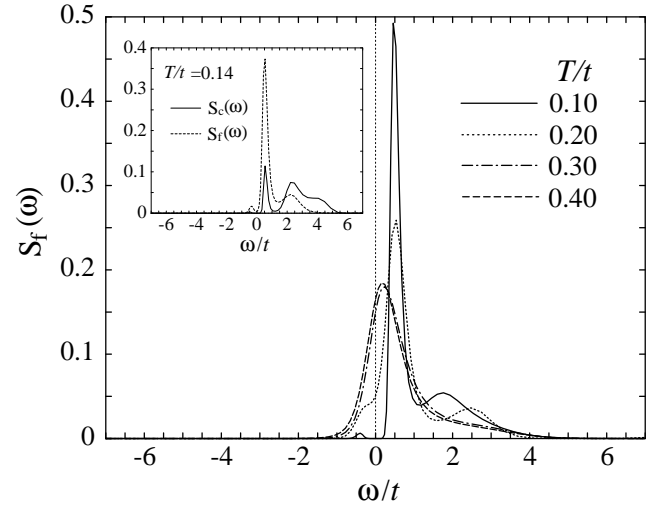


FIG. 21. Dynamic spin structure factor of the f spins, $S_f(\omega)$, of the half-filled one-dimensional Kondo lattice model: $J/t = 1.6$.

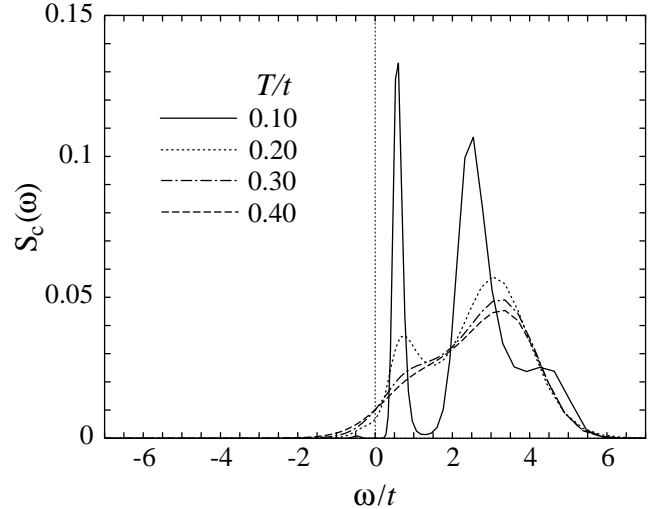


FIG. 22. Dynamic spin structure factor of the conduction electrons, $S_c(\omega)$, of the half-filled one-dimensional Kondo lattice model: $J/t = 1.6$.

The dynamic spin structure factor for the conduction electrons, $S_c(\omega)$, is shown in Fig. 22. At low temperatures, $S_c(\omega)$ has two peaks. The peak in the low frequency side is located at the energy of Δ_s similarly to $S_f(\omega)$. This peak corresponds to the spin excitations of the singlet bound states of conduction electrons with f spins to triplet states. The high frequency peak is located slightly above the charge gap, that corresponds to the spin excitations due to quasiparticles. With increasing the temperature both peaks lose their intensity, and above the temperature $T \sim \Delta_s$ the low frequency peak structure disappears. The spectrum at the high frequency side becomes similar to that of the dynamic charge structure factor $N(\omega)$. This means that high frequency excitations are dominated by the quasiparticle

excitations of almost free conduction electrons and thus the relation $S_c(\omega) = N_c(\omega)/4$ is satisfied approximately.

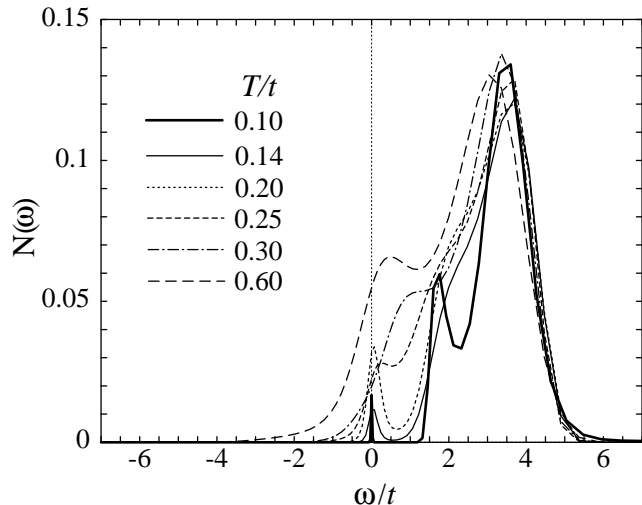


FIG. 23. Dynamic charge structure factor of conduction electrons, $N_c(\omega)$, of the half-filled one-dimensional Kondo lattice model: $J/t = 1.6$.

The dynamic charge structure factor $N(\omega)$ is shown in Fig. 23. At the lowest temperature two clear peaks appear, a smaller peak at $\omega \sim 0$ and a bigger one at Δ_c . These two peaks originate from the sharp peak structure in $\rho(\omega)$ at $\omega = \pm\Delta_{qp}$. The excitations of thermally populated quasiparticles within the sharp peak in $\rho(\omega)$ contribute to the peak at $\omega = 0$, while the excitations between the peaks in $\rho(\omega)$ make the peak in $N(\omega)$ at $\omega \sim \Delta_c$. With increasing temperature, increased number of the thermally populated quasiparticles enhances the peak at $\omega = 0$, but at the temperature $T \sim \Delta_s$ the peak structure is completely smeared out, which reflects the disappearance of the peak in $\rho(\omega)$. The gap structure of $N(\omega)$ and the energy scale of Δ_c become unclear at temperatures much smaller than Δ_c .

Dynamic quantities studied by the finite- T DMRG have revealed the many-body nature of the gap formation in the Kondo insulators. The difference among excitation gaps depending on channels is a characteristic feature of the Kondo insulators compared with the ordinary band insulators. The temperature induced gap formation for the single particle density of states is another clear evidence of the many-body feature. Even at a fixed temperature a renormalized band picture fails to capture the essential physics of the strongly correlated insulators. A typical example is that the two-body excitation spectrum $N(\omega)$ is very different from a convolution of the one-body excitation spectrum $\rho(\omega)$. In the Kondo insulators there are several low energy scales, corresponding to the spin gap, the quasiparticle gap and the charge gap. Among them the lowest one, the spin gap, plays a special role. At higher temperatures than the spin gap, the excitation spectra in the charge sector are also modified strongly. It means that the whole electronic states are reconstructed

above the temperature corresponding to the lowest energy scale.

V. SUMMARY AND DISCUSSIONS

In this review we have discussed Tomonaga-Luttinger liquid properties of the one-dimensional Kondo lattice model away from half-filling. In particular, the large Fermi surface is concluded in the ground state by investigating the spin and charge Friedel oscillations. At half-filling of the one-dimensional Kondo lattice model the ground state is always an incompressible spin liquid phase. Studies on the dynamic correlation functions have revealed many-body nature of this insulating phase in several ways.

These developments have been achieved by applying the density matrix renormalization group method either to the Hamiltonian itself or to the quantum transfer matrix. In the problem of Kondo lattice model there appear small energy scales at low temperatures. It implies that the correlation lengths for various quantities are relatively long and therefore we need sufficiently long systems to observe intrinsic properties. On the other hand, there are 8 states per site in the Kondo lattice problem. Of course for a quantum spin-1/2 chain there are only two states per site. Exact diagonalization studies can do a good job for the latter but only poor one for the former. In this situation the DMRG shows its full advantage for the Kondo lattice model.

We would like to stress that now we can calculate dynamic quantities at finite temperatures by applying the finite- T DMRG to the quantum transfer matrix. This method is free from statistical errors and the truncation errors are the only source of numerical errors. Therefore much better accuracy is obtained for the imaginary time data, from which corresponding spectral function may be obtained reliably through the maximum entropy method. Another advantage of the finite- T DMRG compared with the quantum Monte Carlo simulations is that we do not have the negative sign problem for any quantum systems.

Generally speaking, more elaborate calculations are required for the finite- T DMRG compared with the zero-temperature DMRG. Finite temperature properties, both static and dynamic, of the Tomonaga-Luttinger liquid phase are of great interest and studies in this direction are now being in progress. In near future it will become possible to address these questions. Investigation of a completely Fermionic model for heavy Fermions, for example the periodic Anderson model, is also left for future.

ACKNOWLEDGMENTS

It is our great pleasure to acknowledge fruitful collaborations with Tetsuya Mutou Tomotoshi Nishino, Manfred Sigrist, Matthias Troyer, and Hirokazu Tsunetsugu. We

are also benefitted from discussions with Hiroshi Kontani and Beat Ammon. This work is financially supported by Grant-in-Aid from the Ministry of Education, Science, Sports and Culture of Japan.

[1] J.M. Luttinger, Phys. Rev. **119**, 1153 (1960).
 [2] K. Yosida, Phys. Rev. **147**, 223 (1966).
 [3] M.A. Ruderman and C. Kittel, Phys. Rev. **96**, 99 (1954);
 T. Kasuya, Prog. Theor. Phys. **16**, 45 (1956); K. Yosida,
 Phys. Rev. **106**, 893 (1957).
 [4] H. Tsunetsugu, M. Sigrist, and K. Ueda, Rev. Mod. Phys.
 69, 809 (1997).
 [5] H. Tsunetsugu, Y. Hatsugai, K. Ueda, and M. Sigrist,
 Phys. Rev. **B46**, 3175 (1992).
 [6] S. R. White, Phys. Rev. Lett. **69**, 2863 (1992); Phys.
 Rev. B **48**, 10 345 (1993).
 [7] N. Shibata, J. Phys. Soc. Jpn, **66**, 2221 (1997).
 [8] X. Wang and T. Xiang, Phys. Rev. B**56**, 5061 (1997).
 [9] N. Shibata, B. Ammon, M. Troyer, M. Sigrist and K.
 Ueda, J. Phys. Soc. Jpn **67**, 1086 (1998).
 [10] S. Ostlund and S. Rommer, Phys. Rev. Lett. **75**, 3537
 (1995).
 [11] F.D.M. Haldane, J. Phys. C **14**, 2585 (1981).
 [12] H.J. Schulz, Phys. Rev. Lett. **64**, 2831 (1990).
 [13] N. Shibata, A. Tsvelik, and K. Ueda, Phys. Rev. B**56**,
 330 (1997).
 [14] N. Shibata, K. Ueda, T. Nishino, and C. Ishii, Phys. Rev.
 B **54**, 13495 (1996).
 [15] M. Fabrizio and A. O. Gogolin, Phys. Rev. B **51**, 17827
 (1995).
 [16] R. Egger and H. Grabert, Phys. Rev. Lett. **75**, 3505
 (1995).
 [17] R. Egger and H. Schoeller, Czech. J. Phys. **46**, Suppl. S4,
 1909 (1996).
 [18] K. Ueda, T. Nishino, and H. Tsunetsugu, Phys. Rev.
 B**50**, 612 (1994).
 [19] S. Fujimoto and N. Kawakami, J. Phys. Soc. Jpn. **63**,
 4322 (1994).
 [20] S. R. White and I. Affleck, Phys. Rev. B **54**, 9862 (1996).
 [21] A. E. Sikkema, I. Affleck, and S. R. White, Phys. Rev.
 Lett. **79**, 929 (1997).
 [22] M. Yamanaka, M. Oshikawa, and I. Affleck, Phys. Rev.
 Lett. **79**, 1110 (1997).
 [23] E.B. Kolomeisky and J.P. Straley, Rev. Mod. Phys. **68**,
 175 (1996).
 [24] G. Bedürftig, B. Brendel, H. Frahm, R.M. Noack, cond-
 mat/9805123 (1998).
 [25] C. C. Yu and S. R. White, Phys. Rev. Lett. **71**, 3866
 (1993).
 [26] A. M. Tsvelik, Phys. Rev. Lett. **72**, 1048 (1994).
 [27] S. Fujimoto and N. Kawakami, J. Phys. Soc. Jpn. **66**,
 2157 (1997).
 [28] R. N. Silver, D. S. Sivia, and J. E. Gubernatis, Phys.
 Rev. B **41**, 2380 (1990).
 [29] J. E. Gubernatis, M. Jarrell, R. N. Silver, Phys. Rev. B
 44, 6011 (1991).
 [30] M. Jarrell and J. E. Gubernatis, Phys. Rep. **269**, 133
 (1996). Phys. Rev. Lett. **72**, 1048 (1994).
 [31] T. M. Rice and K. Ueda, Phys. Rev. Lett. **55**, 995 (1985);
 Phys. Rev. B **34**, 6420 (1986).
 [32] J. Igarashi, T. Tonegawa, M. Kaburagi, and P. Fulde,
 Phys. Rev. B **51**, 5814 (1995).
 [33] T. Nishino and K. Ueda, Phys. Rev. B **47**, 12451 (1993).
 [34] E. H. Lieb and F. Y. Wu, Phys. Rev. Lett. **20**, 1445
 (1968).
 [35] T. Mutou, N. Shibata, and K. Ueda, preprint (1998).